Synthesis and characterization of Fe_3O_4-NH_2 and Fe_3O_4-NH_2-chitosan nanoparticles

M. L. D. C. Silveira[1], I. M. B. Silva[1], A. G. Magdalena[1]*

[1]UNESP-São Paulo State University, School of Science, Department of Chemistry, 17033-360, Bauru, SP, Brazil

Abstract

Fe_3O_4 nanoparticles were synthesized and functionalized with (3-aminopropyl) trimethoxysilane (APTMS) and chitosan, forming Fe_3O_4-NH_2 and Fe_3O_4-NH_2-chitosan nanoparticles. The Fe_3O_4 nanoparticles were synthesized by a co-precipitation method and functionalization was performed in further stages. The nanoparticles were characterized by X-ray diffraction (XRD), Fourier transform infrared spectroscopy (FTIR), zeta potential, and transmission electron microscopy (TEM). The results of XRD showed that magnetite did not experience an oxidation reaction. The functionalization of the surface of Fe_3O_4 nanoparticles was confirmed by FTIR and zeta potential measurements. The TEM results showed a thin layer around Fe_3O_4 nanoparticles due to the functionalization with the APTMS. The later functionalization by chitosan contributed to the agglomeration of nanoparticles. Functionalization provided the nanoparticles better colloidal stability mainly for a pH below 7 and this improvement was related to the protection and new functional groups from the APTMS and chitosan.

Keywords: nanoparticles, functionalization, surface modification.

INTRODUCTION

The synthesis of nanoparticles has been the object of several studies [1-8]. In this sense, magnetic nanoparticles with Fe_3O_4 are being extensively studied due to their properties and applications [1, 2, 4, 6, 9]. The applications of these nanoparticles are related to their elevated surface area, low toxicity, chemical affinity, biocompatibility, and magnetic properties [3, 6]. The action of the external magnetic field in magnetic nanoparticles has several applications for these nanoparticles, which have been extensively used in adsorptive and photocatalytic processes and catalysis in general [1, 2, 4, 6, 9]. Additionally, they have been used in biomedicine as a vehicle for transporting medication [9]. This characterizes these nanomaterials as multifunctional materials, which makes them a versatile tool for different areas of knowledge [1, 2, 4, 6, 9].

Different methodologies are used to obtain Fe_3O_4 nanoparticles, among which we can highlight co-precipitation, sol-gel, hydrothermal, microemulsion, and thermal decomposition methods [3, 6]. Among these, the co-precipitation method is the simplest and presents the lowest cost. One of the great limitations of nanoparticles is associated with the colloidal stability of these systems due to the nanometric range of the particles and their instability over time [1, 3, 6]. Therefore, it is a great challenge to develop strategies for the functionalization of nanoparticles to improve colloidal properties and the potential new functionalization of these materials [4, 6, 9]. Another crucial aspect is the contribution to the surface of these materials, adsorption sites, and electronic and geometric structures, considering that such functional groups can interact with magnetite [3, 6]. Nanofibers consisting of magnetite functionalized with an amino group were used as adsorbents for heavy metals such as Pb(II) and Ni(II) [10]. The results obtained were very promising for the adsorption and desorption processes in several cycles of use of these nanomaterials. Some studies have shown that chitosan functionalization by magnetite presented effective systems for the controlled release of drugs [11, 12].

The structure of the APTMS molecule has 3-methoxy groups and it experiences a polymerization reaction in an aqueous solution [13, 14]. The modification of nanoparticle surfaces by APTMS provides the surface of this material the potential for several applications such as environmental remediation and biomedicine, among others [13], because it allows the possibility of other chemical reactions, thus generating multifunctional materials. Chitosan is a polysaccharide with applications in food, agriculture, medicine, and dentistry as a microencapsulating agent in release systems. The great interest in chitosan comes from its abundance, versatility, and chemical characteristics because it has unique properties, including biodegradability, biocompatibility, non-toxicity, hydrophilicity, and antibacterial, antifungal, and wound healing effects [11, 15]. Chitosan has low water solubility but is completely soluble in aqueous solutions of acetic or formic acid. The chemical versatility and new functional properties of chitosan are due to its available functional groups (-NH_2 and -OH) [15]. Chitosan can bind to various compounds such as proteins, cholesterol, metal ions, and drugs, among others [12, 15-17]. Several studies have been published to functionalize the surface of Fe_3O_4 nanoparticles. Knowing the reaction mechanism during the functionalization process

**aroldo.magdalena@unesp.br*

https://orcid.org/0000-0003-3385-2106

is important to understand the potential future reactions of the functionalized nanoparticles. Several studies present the reaction mechanism of the functionalization of Fe_3O_4 nanoparticles with chitosan using glutaraldehyde [18] and sodium polyphosphate [19, 20] as the new cross-linkers and other forms of chitosan functionalization on Fe_3O_4 nanoparticles [21, 22]. Due to the lack of information regarding the use of NaOH as a cross-linking agent in the functionalization mechanism, this study aimed to synthesize and characterize Fe_3O_4 nanoparticles functionalized with APTMS and later with chitosan.

MATERIALS AND METHODS

Materials: the materials used in this study were 98% $FeCl_2.4H_2O$ (Aldrich), 97% $FeCl_3.6H_2O$ (Synth), 25% ammonium hydroxide (NH_4OH, Synth), 97% (3-aminopropyl) trimethoxysilane (APTMS, Aldrich), 75-85% deacetylated low-molecular weight chitosan (Aldrich), 97% sodium hydroxide (NaOH, Dynamic), and 99.7% acetic acid (Synth).

Synthesis and characterization techniques: the Fe_3O_4 nanoparticles were synthesized using the co-precipitation method [8, 11, 12, 15, 16]. For this synthesis, 0.05 mol.L^{-1} $FeCl_3.6H_2O$ and 0.025 mol.L^{-1} $FeCl_2.4H_2O$ solutions were prepared. The precursors were mixed in 300 mL of distilled water and maintained at room temperature and constant agitation under the bubbling of an inert N_2 atmosphere for removing excess oxygen from the solution. After 10 min, NH_4OH was added in drops until reaching a pH of 9.5, showing the formation of a black precipitate. The system was agitated with mechanical stirring at ~200 rpm for 1 h under the bubbling of an inert N_2 atmosphere to prevent the oxidation process of magnetite (Fe_3O_4) nanoparticles [8, 11, 12, 15, 16]. Next, the nanoparticles were separated magnetically and washed with water until reaching a pH close to 7.0. The nanoparticles were dried in a rotary evaporation system at 60 °C. For the synthesis of Fe_3O_4-NH_2, 200 mg of Fe_3O_4 recently synthesized were dispersed in 70 mL of a 1:1 mixture of ethanol-water, and the pH of the system was adjusted to around 8.8 aided by ~25% NH_4OH. Moreover, 100 μL of APTMS was added to the system and left for reacting for 1 h at 40 °C [11]. The nanoparticles obtained were washed with distilled water until reaching a pH of 7.0. The washing and drying procedures were identical to those performed for Fe_3O_4 nanoparticles. In the synthesis procedure of Fe_3O_4-NH_2-chitosan nanoparticles, 200 mg of Fe_3O_4-NH_2 nanoparticles were dispersed in 300 mL of chitosan solution in a 2% acetic acid medium. The mixture was allowed to stir for 1 h. Thereafter, 50 mL of 5 mol.L^{-1} NaOH solution was added dropwise [17]. The washing and drying procedures were identical to those performed for Fe_3O_4 nanoparticles.

Nanoparticle samples were characterized by transmission electron microscopy (TEM) performed with a microscope (CM-200, Philips) with a super twin a-lens; X-ray diffraction (XRD) patterns were obtained with a diffractometer (Rint 2000, Rigaku) with CuKα radiation. The Zetasizer Nano ZS system (Malvern) was also used for the zeta potential measurements; variations in pH were controlled using 0.1 mol.L^{-1} HCl/NaOH solutions in 0.001 mol.L^{-1} NaCl solution. The attenuated total reflectance-Fourier transform infrared (ATR-FTIR) spectra were measured using a spectrometer (Vertex 70, Bruker). The particle size was calculated with analyses of TEM images using the ImageJ software. The scheme of the reaction mechanism was drawn with the ACD/ChemSketch software.

RESULTS AND DISCUSSION

Fig. 1 shows the results of the X-ray diffraction of all samples. The X-ray diffractograms showed no changes in crystallographic planes and the results indicated that Fe_3O_4 nanoparticles did not experience oxidation during the syntheses. A single diffraction peak was observed at 2θ around 20° for chitosan. The XRD pattern of the Fe_3O_4-NH_2-chitosan nanoparticles showed the contribution of chitosan at this 2θ range.

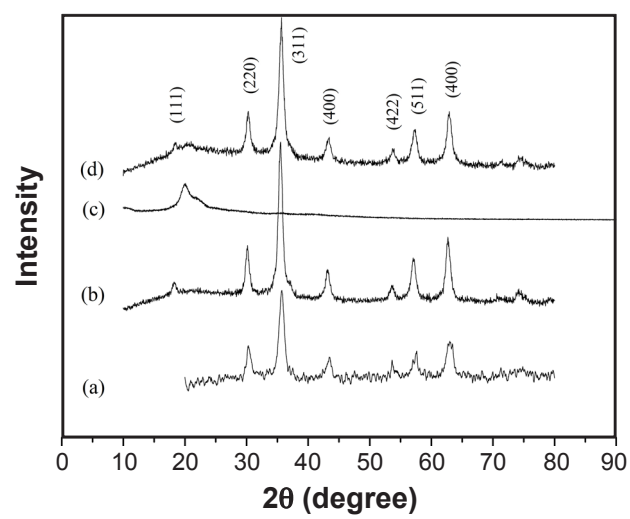

Figure 1: X-ray diffractograms obtained from: a) Fe_3O_4; b) Fe_3O_4-NH_2; c) pure chitosan; and d) Fe_3O_4-NH_2-chitosan. The crystalline planes observed refer to Fe_3O_4 (JCPDS file n° 89-0688).

Fig. 2 presents the Fourier transform infrared (FTIR) spectra for all nanoparticles studied and Table I shows the descriptions of the FTIR bands observed. The Fe_3O_4 nanoparticles (Fig. 2a) showed three main bands at 580, 1610, and 3267 cm^{-1}. The first band was related to the Fe-O bond, the second was due to the absorption of water molecules, and the third was associated with ν(O-H) stretches [8, 11]. The spectrum of Fe_3O_4-NH_2 nanoparticles (Fig. 2b) showed bands in the interval from 996 to 893 cm^{-1}, which were associated with the Si-O and Si-O-H stretches, respectively. Furthermore, it was verified that the stretches of Si-O-Si and C-N bonds were attributed to the 1116 cm^{-1} and 1375 cm^{-1} bands, respectively [11, 18, 19], while the band at around 1613-1520 cm^{-1} was associated with the R-NH_2 bond [11, 19]. Additionally, the bands verified around 2916

and 3174 cm^{-1} were attributed to C-H and ν(O-H) stretches, respectively. The band at the same wavenumber observed for the ν(O-H) stretch (3174 cm^{-1}) may also be attributed to the asymmetrical stretching of the N-H bond [11, 19]. These data confirmed the functionalization of the magnetite surface forming the Fe_3O_4-NH_2 nanoparticles. Fig. 3 shows the representations of the reaction mechanism according to the FTIR data.

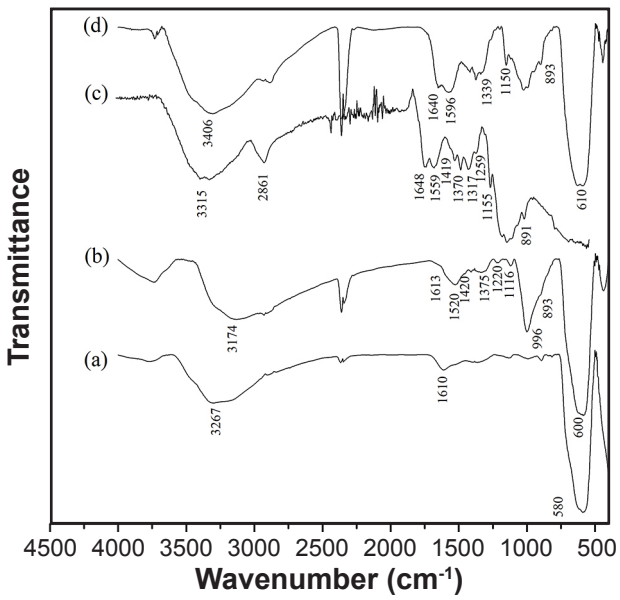

Figure 2: FTIR spectra from nanoparticles: a) Fe_3O_4; b) Fe_3O_4-NH_2; c) pure chitosan; and d) Fe_3O_4-NH_2-chitosan.

Fig. 2c shows the FTIR spectrum of pure chitosan. It was found that the band at around 3315 cm^{-1} was associated with the axial stretch of -OH, which appeared superimposed with the N-H stretch band. The band at the interval from 1639 to 1654 cm^{-1} was due to water adsorption and the axial C=O deformation of the amide. As the degree of acetylation of chitosan is around 75-85%, there should be a contribution from the amide groups. The angular deformation band of N-H was found in the interval from 1580 to 1559 cm^{-1} and the band related to the symmetrical angular deformation of CH_3 and primary alcohol deformation occurred at around 1370 cm^{-1}. The axial deformation of amide -CN occurred at around 1420 cm^{-1} and the deformation of amino groups -CN between 1317 and 1259 cm^{-1}, in addition to bands of polysaccharide structures in the interval of 1190-890 cm^{-1} [23, 24]. For the Fe_3O_4-NH_2-chitosan nanoparticles (Fig. 2d), the bands in the interval from 893 to 1150 cm^{-1} were associated with the stretch of Si-O-Si and the polysaccharide structure of chitosan. The bands in 1339 and 1596 cm^{-1} were due to the C-N and R-NH_2 bonds, respectively. The band verified at around 3406 cm^{-1} was attributed to the ν(O-H) stretches and the asymmetrical stretching of the N-H bond [11, 17]. Additionally, in this spectrum, a central wide band was verified at 1596 cm^{-1}, which may be associated with the R-NH_2 bond and the angular deformation of N-H. A displacement of 76 cm^{-1} was noticed for the 1520 cm^{-1} band of

Table I - Description of FTIR band assignments of the spectra shown in Fig. 2.

Fe_3O_4	Fe_3O_4-NH_2	Pure chitosan	Fe_3O_4-NH_2-chitosan
3267 cm^{-1} ν(O-H stretch)	3174 cm^{-1} ν(O-H stretch and N-H bond)	3315 cm^{-1} ν(O-H stretch and N-H bond)	3406 cm^{-1} ν(O-H stretch and N-H bond)
-	2916 cm^{-1} (C-H stretch)	-	-
1613 cm^{-1} (adsorption of water molecule)	1613-1520 cm^{-1} (R-NH_2 bond)	1654-1639 cm^{-1} (adsorption of water molecule and axial C=O deformation of amide)	1596 cm^{-1} (R-NH_2 bond)
-	-	1580-1559 cm^{-1} (angular deformation band of N-H)	-
-	-	1420 cm^{-1} (axial deformation of amide -CN)	-
-	1375 cm^{-1} (C-N stretch)	1370 cm^{-1} (symmetrical angular deformation of CH_3 and primary alcohol deformation)	1339 cm^{-1} (C-N stretch)
-	-	1317-1259 cm^{-1} (deformation of amino group -CN)	-
-	1116 cm^{-1} (Si-O-Si stretch)	-	-
-	-	1190-890 cm^{-1} (polysaccharide structure)	-
-	996-893 cm^{-1} (Si-O and Si-O-H stretches)	-	1150-893 cm^{-1} (Si-O-Si stretch and polysaccharide structure)
580 cm^{-1} (Fe-O)	600 cm^{-1} (Fe-O)	-	610 cm^{-1} (Fe-O)

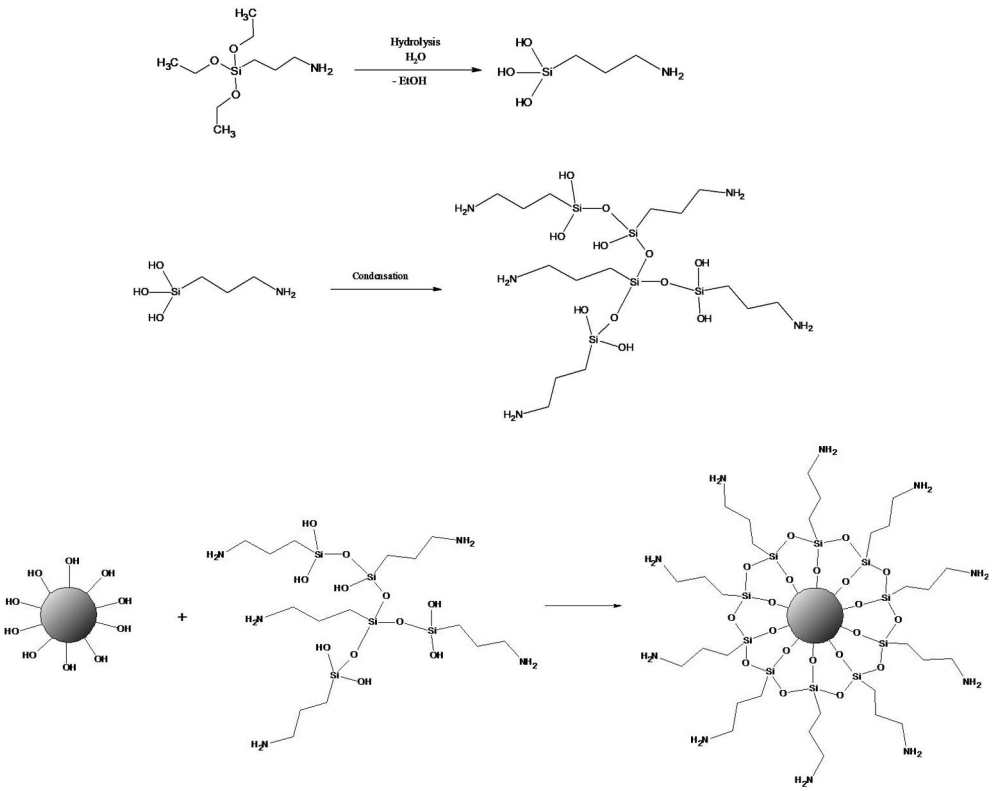

Figure 3: Schemes of the reaction mechanism for the formation of Fe_3O_4-NH_2 nanoparticles (drawn with ACD/ChemSketch software).

Fe_3O_4-NH_2 nanoparticles to 1596 cm^{-1}, which was associated with the angular deformation of N-H and the disappearance of the band associated with the chitosan alcohol stretch (1370 cm^{-1}) [17]. This result indicated a chemical bond of the amino group of Fe_3O_4-NH_2 nanoparticles to the alcohol group of Fe_3O_4-chitosan nanoparticles in an SN_2 substitution reaction, forming the Fe_3O_4-NH_2-chitosan nanoparticles. Fig. 4 shows the schematic representations of the reaction mechanism according to the FTIR data. These results confirmed that the magnetic core was not modified chemically in all samples studied. Moreover, from the functionalization of these samples, the Fe_3O_4 nanoparticles start to present new functional groups such as those visualized in the FTIR spectra. The proposal of the schemes agrees with the FTIR data shown in Fig. 2.

Fig. 5 shows the TEM images of the samples studied, which were obtained with different magnifications. These images show nanoparticulate systems. The TEM image of Fe_3O_4-NH_2 (Fig. 5b) shows a small layer around the Fe_3O_4 nanoparticles due to the functionalization with the APTMS, which is indicated by arrows. This confirmed the mechanism proposed in Fig. 3. Fig. 5c shows that the incorporation of chitosan led to the formation of the agglomerate due to the binding and reticulation of chitosan around the nanoparticles forming the Fe_3O_4-NH_2-chitosan nanoparticles. This was according to Fig. 4. The results showed that the nanoparticles studied presented sizes in the interval from 13 to 16 nm verified by TEM. The nanoparticles of m-Fe_3O_4-CNs prepared by ionic gelation [19] showed morphologies that depended on the proportion between chitosan and polyphosphate. The sizes ranged from 139 to 85 nm. It was observed that the size of particles led to the agglomeration of Fe_3O_4 nanoparticles due to surface energy and it was possible to observe a thin layer of chitosan on the nanoparticle (NP) aggregates. The

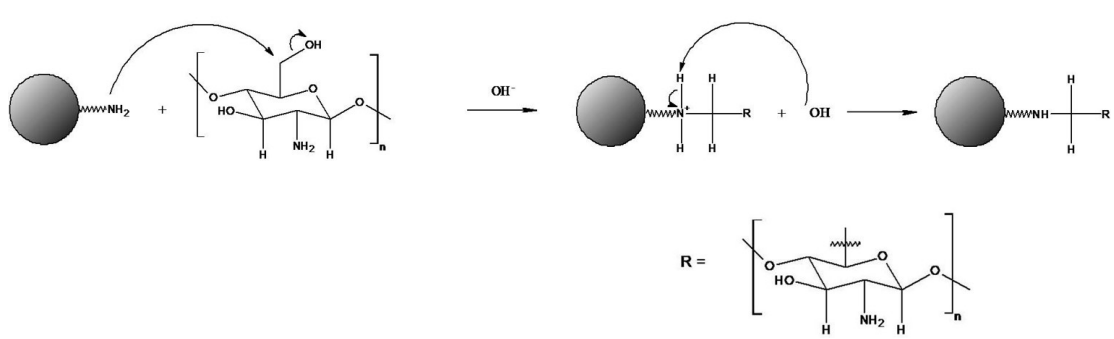

Figure 4: Schemes of the reaction mechanism for the formation of the Fe_3O_4-NH_2-chitosan nanoparticles (drawn with ACD/ChemSketch software).

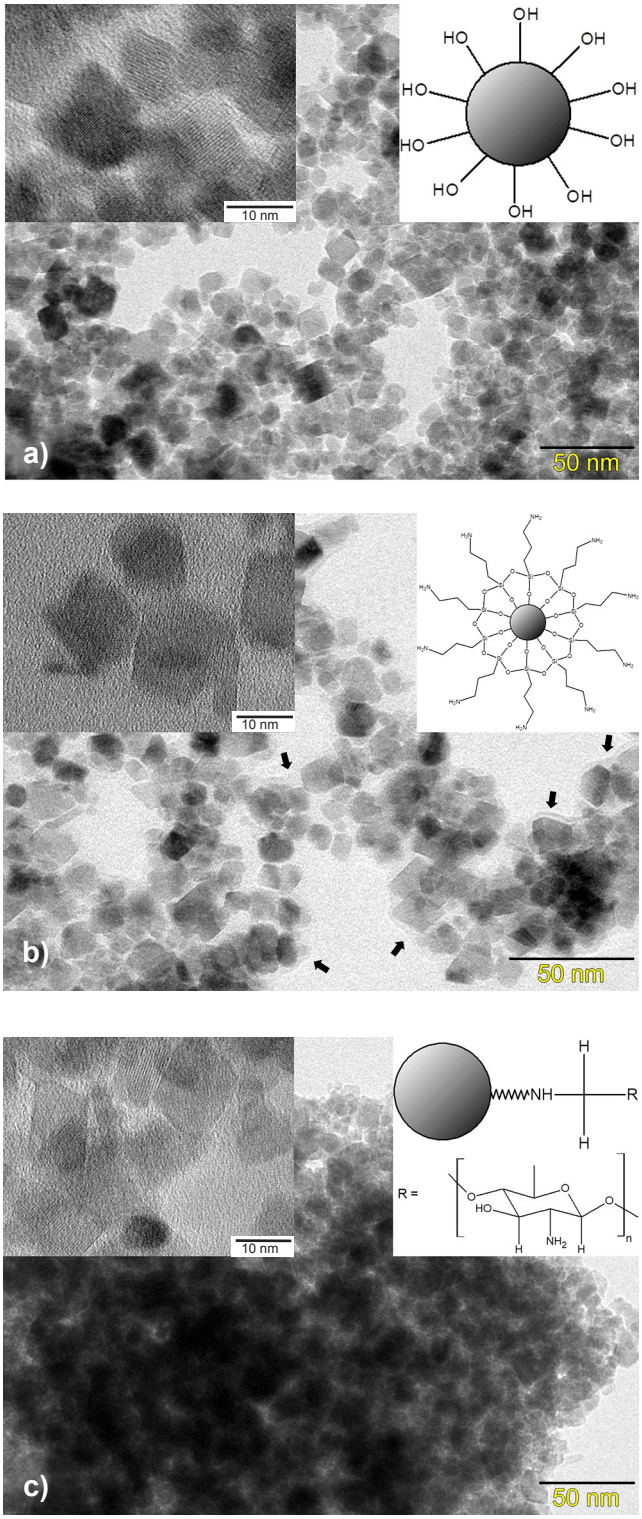

Figure 5: TEM micrographs with different magnifications of nanoparticles of: a) Fe_3O_4; b) Fe_3O_4-NH_2; and c) Fe_3O_4-NH_2-chitosan. Schematic structures elucidated by FTIR in Figs. 3 and 4 are shown on the images

agglomeration of Fe_3O_4 nanoparticles was also observed in our results. However, our results did not show the chitosan layer as seen by Akin et al. [19], so the chitosan probably contributed. In another study [21], after the dissolution of chitosan in a nitric acid medium, Fe_3O_4 NPs were added, and cross-linking was performed with the addition of 30% NH_4OH dropwise; the authors observed that the link between Fe_3O_4 and chitosan occurred between the -OH groups of NPs and the -NH_2 group of chitosan. Our results differed because the interaction with chitosan occurred between the NH_2 group of the Fe_3O_4-NH_2 nanoparticles and the OH group of chitosan. The FTIR data in Fig. 2 support this interpretation.

Another way of analyzing the surface of nanoparticles is from zeta potential measurements. The graph in Fig. 6 shows the zeta potential results as a function of the pH for all nanoparticles studied. These results showed that magnetite functionalization caused a displacement of the point of zero charge to higher pH values, from 6.2 for Fe_3O_4 to 8.3 and 8.7, respectively, for Fe_3O_4-NH_2 and Fe_3O_4-NH_2-chitosan nanoparticles. These results agreed with the literature because, after functionalization, the sample surfaces presented the amino group [25]. Moreover, it may be verified that at pH lower than 6.0, the Fe_3O_4-NH_2-chitosan nanoparticles presented higher colloidal stability than Fe_3O_4 and Fe_3O_4-NH_2 nanoparticles.

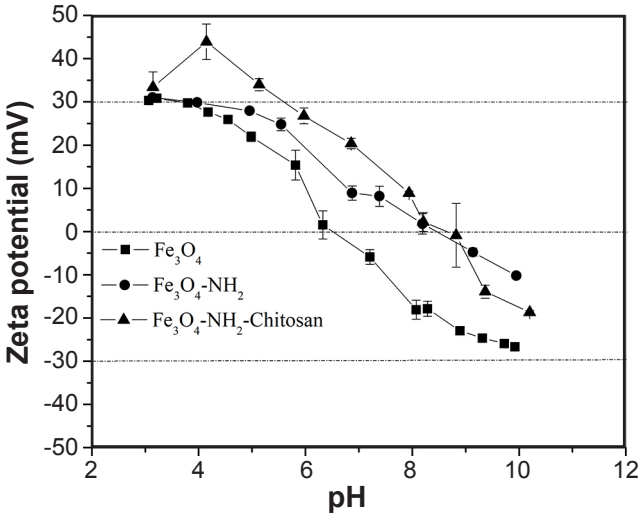

Figure 6: Zeta potential measurements versus pH for the obtained nanoparticles.

The synthesis of Fe_3O_4 nanoparticles by the co-precipitation method proved to be efficient, the XRD data showed that magnetite did not experience an oxidation reaction ($Fe_3O_4 \rightarrow \gamma$-$Fe_2O_3$ or α-Fe_2O_3), and there was no evidence of oxidation of the nanoparticles. Functionalization provided the nanoparticles better colloidal stability, mainly for the pH below 7 and this improvement was related to the protection and new functional groups from the APTMS and chitosan groups. The new functional groups due to the functionalization of nanoparticles can now serve for several applications such as adsorbents, drug carriers, and other potential uses.

CONCLUSIONS

The results showed that the nanoparticles studied

presented sizes in the interval from 13 to 16 nm verified by transmission electron microscopy, and the functionalization of the surface of Fe_3O_4 nanoparticles was confirmed by Fourier transform infrared spectroscopy and zeta potential measurements. The X-ray diffraction results showed that magnetite did not experience an oxidation reaction. Moreover, the results showed a displacement of the point of zero charge to higher pH values for the functionalized nanoparticles associated with the amino group available. Additionally, it was verified that at pH below 6.0 the Fe_3O_4-NH_2-chitosan nanoparticles presented higher colloidal stability than Fe_3O_4 and Fe_3O_4-NH_2 nanoparticles. The proposed reaction mechanisms of the formation of nanoparticles agreed with the experimental results obtained.

ACKNOWLEDGMENTS

The authors would like to thank the São Paulo Research Foundation (FAPESP) and the Brazilian Council for Scientific and Technological Development (CNPq). In particular, we would like to acknowledge CEPID/CDMF - Proc. FAPESP N° 2013/07296-2.

REFERENCES

[1] A. Akbarzadeh, M. Samiei, S. Davaran, Nanoscale Res. Lett. **7**, 1 (2012) 144.
[2] M. Gonçalves, C.S. Castro, A. Oliveira, M.S. Guerreiro, Quím. Nova **32**, 7 (2009) 1723.
[3] A.K. Gupta, M. Gupta, Biomaterials **26**, 18 (2005) 3995.
[4] R. Hao, R. Xing, Z. Xu, Y. Hou, S. Gao, S. Sun, Adv. Mater. **22**, 25 (2010) 2729.
[5] I. Hussain, N.B. Singh, A. Singh, H. Singh, S.C. Singh, Biotechnol. Lett. **38** (2016) 545.
[6] A.-H. Lu, E.L. Salabas, F. Schüth, Angew. Chem. Int. Ed. **46**, 8 (2007) 1222.
[7] N.D. Kandpal, N. Sah, R. Loshali, R. Joshi, J. Prasad, J. Sci. Ind. Res. **73** (2014) 87.
[8] A.G. Magdalena, I.M.B. Silva, R.F.C. Marques, P.N. Lisboa-Filho, M. Jafelicci Jr., J. Phys. Chem. Solids **113** (2018) 5.
[9] L.H. Reddy, J.L. Arias, J. Nicolas, P. Couvreur, Chem. Rev. **112**, 11 (2012) 5818.
[10] M. Jafarnejad, M.D. Asli, F.A. Taromi, M. Manoochehri, Int. J. Biol. **148**, 1 (2020) 201.
[11] M.M. Islam, M. Shahruzzaman, S. Biswas, M. Nurus Sakib, T.U. Rashid, Bioact. Mater. **5**, 1 (2020) 164.
[12] P. Gentile, V.K. Nandagiri, J. Daly, V. Chiono, C. Mattu, C. Tonda-Turo, G. Ciardelli, Z. Ramtoola, Mater. Sci, Eng. C **59**, 1 (2016) 249.
[13] G. Jaksa, B. Stefane, J. Kovac, Appl. Surf. Sci. **315**, 1 (2014) 516.
[14] M. Zhu, M.Z. Lerum, W. Chen, Langmuir **28**, 1 (2012) 416.
[15] B. Fonseca-Santos, M. Chorilli, Mater. Sci. Eng. C **77**, 1 (2017) 1349.
[16] A. Aguilar, N. Zein, E. Harmouch, B. Hafdi, F. Bornert, D. Offner, F. Clauss, F. Fioretti, O. Huck, N. Benkirane-Jessel, G. Hua, Molecules **24**, 16 (2019) 3009.
[17] P. He, S.S. Davis, L. Illum, Int. J. Pharm. **166**, 1 (1998) 75.
[18] A. Kadam, J. Jang, S.R. Lim, D.S. Lee, Theor. Found. Chem. Eng. **54**, 4 (2020) 655.
[19] D. Akin, A. Yakar, U. Gündüz. Water Environ. Res. **87**, 5 (2015) 425.
[20] C. Zhao, X. Liu, X. Zhang, H. Yan, Z. Qian, X. Li, Z. Ma, Q. Han, C. Pei, Mater. Sci. Eng. C **77** (2017) 1182.
[21] E. Asgari, A. Sheikhmohammadi, J. Yeganeh, Int. J. Biol. Macromol. **164** (2020) 694.
[22] M. Meshvardoostchokami, M. Majidi, A. Zamani, B. Liu, J. Mol. Liq. **323** (2021) 115064.
[23] S. Laurent, D. Forge, M. Port, A. Roch, C. Robic, L.V. Elst, R.N. Muller, Chem. Rev. **108**, 6 (2008) 2064.
[24] C.L. Warner, R.S. Addleman, A.D. Cinson, T.C. Droubay, M.H. Engelhard, M.A. Nash, W. Yantasee, M.G. Warner, ChemSusChem **3**, 6 (2010) 749.
[25] R. Bini, R.F.C. Marques, F.J. Santos, J.A. Chaker, M. Jafelicci Jr, J. Magn. Magn. Mater. **324**, 4 (2012) 534.
(Rec. 04/11/2020, Rev. 14/01/2021, 16/02/2021, Ac. 20/02/2021)